Bioorganic & Medicinal Chemistry Letters 23 (2013) 4511–4516

Contents lists available at SciVerse ScienceDirect

Bioorganic & Medicinal Chemistry Letters

journal homepage: www.elsevier.com/locate/bmcl

Discovery of 7-aminofuro[2,3-*c*]pyridine inhibitors of TAK1: Optimization of kinase selectivity and pharmacokinetics

Keith R. Hornberger *, Xin Chen, Andrew P. Crew, Andrew Kleinberg, Lifu Ma, Mark J. Mulvihill, Jing Wang, Victoria L. Wilde, Mark Albertella, Mark Bittner, Andrew Cooke, Salam Kadhim, Jennifer Kahler, Paul Maresca, Earl May, Peter Meyn, Darlene Romashko, Brianna Tokar, Roy Turton

OSI Pharmaceuticals LLC, 1 Bioscience Park Drive, Farmingdale, NY 11735, USA

ARTICLE INFO

Article history:
Available online 27 June 2013

Keywords:
TAK1
Inhibitors
7-Amino-furo[2,3-*c*]pyridine
Cancer
Inflammation

ABSTRACT

The kinase selectivity and pharmacokinetic optimization of a series of 7-aminofuro[2,3-*c*]pyridine inhibitors of TAK1 is described. The intersection of insights from molecular modeling, computational prediction of metabolic sites, and in vitro metabolite identification studies resulted in a simple and unique solution to both of these problems. These efforts culminated in the discovery of compound **13a**, a potent, relatively selective inhibitor of TAK1 with good pharmacokinetic properties in mice, which was active in an in vivo model of ovarian cancer.

In the preceding article,[1] we reported on the discovery and initial optimization of a potent series of 7-aminofuro[2,3-*c*]pyridines as inhibitors of transforming growth factor β receptor-associated kinase 1 (TAK1 or MAP3K7), resulting in identification of the potent lead compounds **1a**, **1b**, and **1c** (Fig. 1). These early tool compounds, however, were relatively multi-targeted kinase inhibitors and also displayed sub-optimal pharmacokinetic properties in mice. We thus felt they were unsuitable for validating the potential for TAK1 inhibition to be useful in the treatment of cancer or inflammatory diseases. Herein we report a concise solution to both of these problems, culminating in the discovery of tool compound **13a**, which showed activity in an in vivo model of ovarian cancer.

Optimization of the kinase inhibitory profile of a given chemical series from a multi-targeted profile toward a more selective profile is by its nature a highly multivariate problem. There are over 500 kinases in the human kinome,[2] and it is generally not feasible or cost-effective to screen the entire kinome with full dose–response curves against even a single compound. Furthermore, there is typically an upward shift when kinase inhibitory activity is evaluated in cells, reflective of both the more complicated cellular milieu and the much higher ATP concentration in cells relative to the K_m for ATP for most kinases.[3,4] Thus, biochemical inhibition does not always linearly translate into cellular inhibition and true consequences in vivo. At the outset, we screened compounds at a single concentration in a broad panel of 192 kinases in a mobility shift assay and then conducted follow-up cellular mechanistic screening on kinases known to have toxicity concerns and/or the potential to confound efficacy readouts. Medicinal chemistry efforts were then focused on removing activity against kinases of concern, with the aspiration that the overall selectivity profile would be improved in the process.

In the in-house 192 kinase panel, compound **1a** inhibited 42/192 kinases >50% at 250× TAK1 K_i, indicating a relatively multi-targeted profile. Other compounds closely related to **1b** and **1c** showed comparable results, indicating a more widespread kinase selectivity issue within the chemotype. Among the 42 kinases registering as hits in the panel were two of particular concern for cellular follow-up: Aurora B and KDR/VEGFR2. Aurora B is a cell cycle kinase which has critical functions in mitosis and has been the subject of intense preclinical and clinical investigation for the treatment of cancer.[5] Aurora family inhibitors can, however,

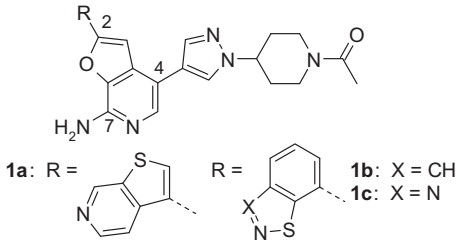

Figure 1. Representative 7-aminofuro[2,3-*c*]pyridine leads from early optimization efforts.

* Corresponding author at present address: Boehringer Ingelheim Pharmaceuticals, 900 Ridgebury Road, Ridgefield, CT 06877, USA. Tel.: +1 203 798 5137; fax: +1 203 791 6072.
E-mail address: keith.hornberger@boehringer-ingelheim.com (K.R. Hornberger).

0960-894X/$ - see front matter © 2013 Elsevier Ltd. All rights reserved.
http://dx.doi.org/10.1016/j.bmcl.2013.06.054

be thought of as 'targeted cytotoxics' and such activity has the potential for both dose-limiting neutropenia[5] and contributing to non-TAK1-mediated efficacy. KDR is a clinically validated target for oncology, with multiple inhibitors approved for treatment of renal cell carcinoma.[6] However, KDR inhibition also is associated with hypertension clinically[7] and could further confound efficacy readouts by inhibition of tumor angiogenesis. Both activities were deemed of enough concern that the medicinal chemistry campaign focused on the removal of these activities in the cellular setting.

Examination of the previously acquired X-ray crystal structure of **1c** (Fig. 2) in the TAK1–TAB1 fusion protein highlighted two potential areas where selectivity inroads could be made. S111 in the ribose pocket of TAK1 corresponds to E161 of Aurora B, suggesting that a substituent reaching into the ribose pocket and clashing with the larger E161 would improve selectivity. V42 of TAK1, at the beginning of the P loop, corresponds to L838 in KDR and forms the top of a relatively narrow channel that the 4-pyrazole substituent fits through. Although this Val versus Leu difference was relatively small, we felt that introduction of some torsion to the 4-substituent, which was nearly coplanar with the furopyridine core in **1c** (dihedral angle ~4°), could improve KDR selectivity. Conceptually, replacing the pyrazole with a larger ring or introducing a substitution at the pyrazole 3- or 5-position should (a) cause increased steric repulsion with the furopyridine core C3 proton to introduce torsion and (b) reach further into the ribose binding pocket, potentially affording selectivity for both Aurora B and KDR simultaneously.

Compounds exploring this concept were synthesized as outlined in Scheme 1. Beginning from the previously described[1] compound **2**, Suzuki coupling with the appropriate boronic ester (**3**) installed the 2-substituent as in **4**, which was then iodinated (**5**) and transformed to final analogs (**6**) via a second Suzuki coupling. For a few compounds where the coupling partners were not readily accessible, it was necessary to reverse the nucleophile/electrophile partners in the coupling event. Compound **5** was thus Boc protected and converted to the corresponding stannane (**7**), which allowed some additional analogs to then be prepared by successive Stille coupling and Boc deprotection. One acetylenic analog (**6m**) was accessed by Sonogashira coupling from **5**.

A survey of the initial 4-position SAR (Table 1) showed that the 4-pyrazole substituent (**6a**) analogous to that from the early high-throughput screening hits was the optimal platform to conduct further selectivity explorations from, with most other five-membered and all six-membered cyclic substituents showing significantly reduced TAK1 activity. The linear linker typified by acetylene **6m** also lost substantial TAK1 activity. Although a thiazole 4-substituent (**6i**) was also relatively potent against TAK1, it offered no advantage in overall physicochemical properties or lipophilic ligand efficiency[8] (LLE = 6.2 for **6a** vs LLE = 5.7 for **6i**) and was deprioritized for further follow-up.

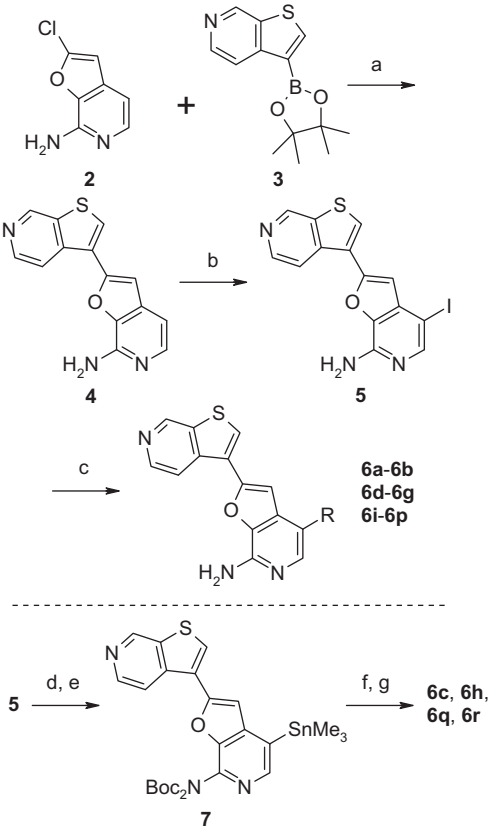

Scheme 1. Preparation of 4-substituted analogs **6**. Reagents and conditions: (a) $PdCl_2dppf$, K_2CO_3, 1,4-dioxane/H_2O, reflux (79%); (b) NIS, DMF, rt (77%); (c) R-$B(OH)_2$ or R-B(pin), $PdCl_2dppf$, K_2CO_3, 1,4-dioxane/H_2O, 80–100 °C, μW or $Pd(PPh_3)_4$, CuI, Et_3N, THF/DMF, 40 °C (for **6m**); (d) Boc_2O, DMAP, toluene/DMF, 50 °C; (e) $Me_3SnSnMe_3$, $Pd(PPh_3)_4$, toluene, 120 °C (89%, 2 steps); (f) R-I or R-Br, Pd_2dba_3, P(*o*-tolyl)$_3$, Et_3N, DMF, 70 °C; (g) 4 N HCl, 1,4-dioxane, rt.

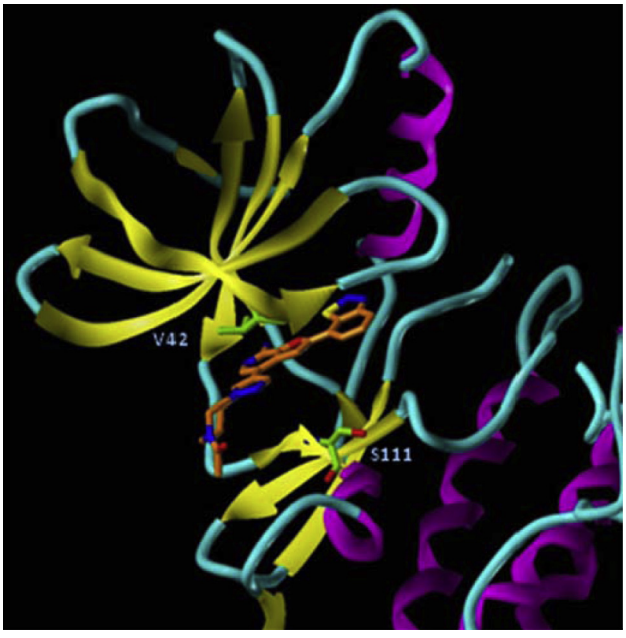

Figure 2. Potential selectivity sites for Aurora family kinases and KDR/VEGFR2.

Focusing attention more closely on the furopyridine 4-pyrazole substituent, we briefly explored a palette of 3- and 5-substitutions on the pyrazole ring itself, with the anticipation that 3-substitution, facing into the ribose binding pocket, would deliver enhanced selectivity for Aurora B and KDR. Cellular inhibition of Aurora B was tracked by measuring inhibition of histone H3 S10 phosphorylation (pHH3) in HT-29 cells, as this histone site is characterized to be phosphorylated by Aurora B.[5] Cellular inhibition of KDR was tracked by measuring inhibition of KDR autophosphorylation in VEGF-stimulated HEK293 cells overexpressing KDR. Unfortunately, we observed a substantial TAK1 potency loss from both simple 3-methyl (**6n**) and 5-methyl (**6o**) pyrazole substitutions, effects which were additive in combination (**6p**). The poor tolerance of the 5-methyl was anticipated due to a steric clash with the proximal Y106 of TAK1, immediately adjacent to the hinge binding residues. The loss of activity with 3-substitution is less easily rationalized; presumably the introduced torsion precluded an adequate fit to the narrow channel the pyrazole occupies in TAK1. A 3-methoxy substituent (**6q**) was better tolerated, but there was still a four-fold loss in activity versus the unsubstituted compound. A

Table 1
SAR of 4-substitutions

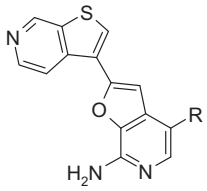

Compd	R	IC_{50}[a] (μM)	Compd	R	IC_{50}[a] (μM)
6a	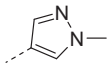	0.15	**6h**		1.4
6b	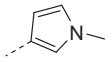	4.9	**6i**	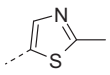	0.23
6c		12.7	**6j**		3.2
6d		0.56	**6k**		3.8
6e	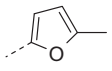	2.1	**6l**	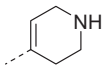	23.6
6f		2.2	**6m**	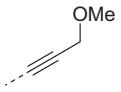	2.9
6g	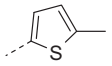	4.6			

[a] Biochemical ALPHAScreen assay with TAK1–TAB1 fusion protein in the presence of 100 μM ATP; values are the mean of ⩾2 experiments.

more rigid 3-cyano substituent (**6r**) was not tolerated. Compound **6n** offered some signs of improved cellular selectivity for Aurora B and KDR, validating the initial design concept. In the final analysis, however, the loss of TAK1 activity suffered by these compounds was deemed too great for use as potential tools and further evolution of this SAR was also deprioritized (Table 2).

In parallel with this initial exploration of the kinase selectivity SAR, we also evaluated the pharmacokinetic properties of our lead compounds and attempted to tune physicochemical properties by modulation of the solvent-exposed pyrazole N-substitution. Although we conducted an extensive medicinal chemistry effort around pyrazole N-substitution, potency and selectivity SAR were relatively flat and therefore only key pharmacokinetic observations for representative compounds are detailed here (Table 3). First, we noted that the thienopyridine 2-substituent had inferior bioavailability relative to other lead structures (compare **1a** and **1b**). Second, replacement of the pyrazole *N*-acetyl piperidine substitution with a cyclohexanol resulted in further improvement in oral bioavailability (compare **1b** and **1d**). Finally, the benzothiadiazole 2-substitution had the best overall oral exposure (compare **1d** and **1e**). Compound **1e** had a late oral t_{max} = 8 h with a second, lower peak concentration at 2 h, together indicative of potential enterohepatic recycling.[9] This observation may afford a rationale for the apparent >100% bioavailability. Based on these pharmacokinetic results, we therefore shifted our future SAR focus to the benzothiadiazole 2-substituent (chemotype **C**) and cyclohexanol pyrazole N-substituent (chemotype **E**).

While we had made gains in oral bioavailability as a result of this exploration, setting aside the substantial potential contributions from enterohepatic recycling, the absolute oral area under

Table 2
SAR of 4-pyrazole substitutions

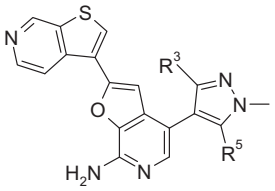

Compd	R^3	R^5	IC_{50}[a] (μM)			
			TAK1[b]	pJNK[c]	pHH3[d]	pKDR[e]
6a	H	H	0.15	0.19	3.0	3.4
6n	Me	H	3.5	1.0	>20	>20
6o	H	Me	4.1	3.0	17.4	19.9
6p	Me	Me	23.9	4.4	NT	NT
6q	OMe	H	0.60	1.7	>20	>20
6r	CN	H	22.8	>10	NT	NT

[a] Values are the mean of ⩾2 experiments; NT = not tested.
[b] Biochemical ALPHAScreen assay with TAK1–TAB1 fusion protein in the presence of 100 μM ATP.
[c] Inhibition of JNK phosphorylation in TNFα-stimulated HCT-116 cells.
[d] Inhibition of histone H3 (HH3) S10 phosphorylation in HT-29 cells.
[e] Inhibition of KDR autophosphorylation in HEK293/KDR cells.

Table 3
Mouse pharmacokinetic parameters for selected compounds

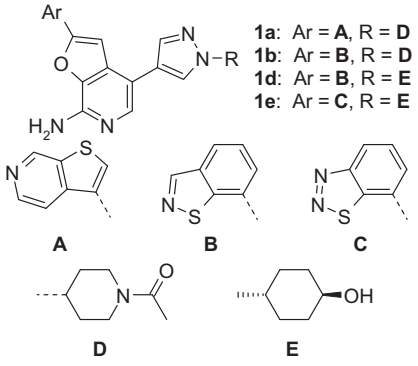

Route	Parameters	1a	1b	1d	1e
iv[a]	Cl (mL/min/kg)	178	128	111	70
	$t_{½}$ (h)	0.1	0.5	3.3	1.6
	$AUC_{0-\infty}$ (ng h/mL)	187	261	299	477
	V_{ss} (L/kg)	2.5	2.5	12	4.1
p.o.[b]	C_{max} (μM)	0.03	1.6	1.1	7.8
	$AUC_{0-\infty}$ (ng h/mL)	21[c]	285	821	16,003
	F (%)	1	11	27	335

[a] iv PK dosed at 2 mg/kg.
[b] p.o. PK dosed at 20 mg/kg.
[c] AUC_{0-last}; compound was below the limit of quantitation at 8 h after oral administration and $AUC_{0-\infty}$ was not calculated.

the curve (AUC) and concentration–time profile were still suboptimal for all of these compounds. A major factor hampering these chemotypes was that all had high systemic clearance, and we anticipated that little further progress would be made on improving pharmacokinetics without understanding and reducing compound metabolism. A computational analysis of compounds **1a** and **1e** for sites of CYP metabolism using the StarDrop program[10] identified few clear leads. The thienopyridine sulfur of **1a** was predicted to be highly labile, but this potential metabolic site was already corrected for in **1e**. Compound **1e** itself had no highly

labile sites identified that would alone explain its high clearance. We also conducted an in vitro metabolite identification study on **1a** in mouse and human liver microsomes in the presence of both NADPH and UDPGA cofactors. Although several minor oxidative metabolites were detected, the common major metabolite was an M+176 metabolite corresponding to a single glucuronidation. Suspecting this glucuronidation to be occurring on the furopyridine 7-amino substituent, we also ran metabolite identification on the 7-des-amino counterpart of **1a** and observed that the glucuronide metabolite had completely disappeared. A glucuronide metabolite also aligned with the apparent >100% bioavailability of **1e**; depot of glucuronides in bile followed by cleavage and recirculation of the parent compound in the intestine is a known mechanism for enterohepatic recycling.[9]

Although we now had a clear sense of the major site of metabolism within the chemical series, this was a particularly vexing medicinal chemistry problem due to the essential function of the 7-amino group in anchoring binding to the hinge of TAK1. Accepting that we could not remove the 7-amino group altogether, we instead wondered whether it would be possible to modulate its nucleophilicity, for example by attachment of an electron-withdrawing group to an open site on the furopyridine core. These hypotheses around metabolism were coming to the fore just as the kinase selectivity exploration around the pyrazole 4-substituent was concluding and we were concomitantly seeking alternate ways to achieve Aurora B and KDR selectivity. We realized that the furopyridine 3-position offered an opportunity to solve both the metabolism and kinase selectivity problems in a single stroke. In addition to providing a venue for anchoring an electron-withdrawing group for metabolic stability, the 3-position also directly faces the ribose binding pocket of TAK1. Such a 3-substitution could thus provide the desired steric clash with E161 of Aurora B and introduce torsion to the pyrazole 4-substituent for KDR selectivity. The only remaining obstacle in reduction of this strategy to practice was the synthesis of the 3-substituted compounds.

At this point we also realized that the means to achieve such a synthesis were already within reach (Scheme 2). Previously[1] we reported the synthesis of compound **8** as a by-product of the desired C2 mono-chlorination of the furopyridine core en route to compound family **1** and **6**. Ironically, this by-product, initially perceived to be a synthetic nuisance requiring painstaking chromatographic separation, now became the linchpin of the synthetic campaign for the core 3-substitution.[11] Compound **8** was deprotected under acidic conditions to **9**, iodinated (**10**) with NIS, and then transformed to **11** and **12** by a series of sequential Suzuki couplings analogous to that used for compound series **1**. Global removal of all protecting groups afforded the 3-Cl substituted compound **13a**, and coupling of this chloride with zinc cyanide in turn gave **13b**. For the preparation of all other compounds, it was necessary to Boc protect the 7-amino group to give **14**. Various heterocyclic substituents (**13c**, **13d**) could be accessed by Suzuki coupling, although substantial optimization of conditions was needed to affect coupling of this sterically congested aryl chloride.[12] Some fluorinated analogs (**13e**, **13f**) were accessed by Suzuki coupling of a vinyl group, followed by ozonolysis with either PPh_3 or $NaBH_4$ work-up, and then subsequent fluorination with DeoxoFluor.

The SAR of the furopyridine 3-substituted compounds **13** is described in Table 4. In general, most compounds demonstrated good maintenance of TAK1 biochemical and cellular potency, although a larger 6-membered heterocyclic substituent (**13c**) displayed some loss of activity. All of the 3-substituted compounds traded back some lipophilic ligand efficiency, but the loss was deemed necessary to address the other deficits of the chemotype. Gratifyingly, most compounds demonstrated enhanced cellular selectivity for Aurora B and especially KDR compared to **1e**. In particular, compound **13a** showed an excellent balance of TAK1 activity and kinase cellular selectivity (>300× for Aurora B and >1000× for KDR). We also evaluated compound **13f** against the broader biochemical panel of 192 kinases and confirmed that as selectivity for Aurora B and KDR improved, so too did the overall selectivity profile. At ~50× TAK1 K_i, **13f** showed >50% inhibition for only 4/192 kinases in the panel: $FLT3^{D835Y}$, HGK, MAP4K5, and MINK1. We further obtained an X-ray crystal structure of **13a** bound to TAK1–TAB1 fusion protein (Fig. 3) and found that it possessed exactly the features hypothesized to enhance selectivity. The single largest change in this structure compared to the earlier structure of **1c** was the increased dihedral angle between the furopyridine core and the 4-pyrazole substituent (~25° vs ~4° in **1c**), bringing the pyrazole C5 ~1 Å closer to the selectivity residue V42 (L838 in KDR).

Equally gratifying was that the majority of the 3-substituted analogs had somewhat reduced extraction ratios in mouse and human liver microsomes compared to **1e**. However, our microsomal preparations were not run in the presence of the cofactors needed for Phase II metabolism, for example UDPGA, and thus may not fully capture the impact of the 3-substitutions on glucuronidation. Indeed, the mouse pharmacokinetics of **13a** and **13f** (Table 5) were dramatically improved compared to **1e**. Both compounds had

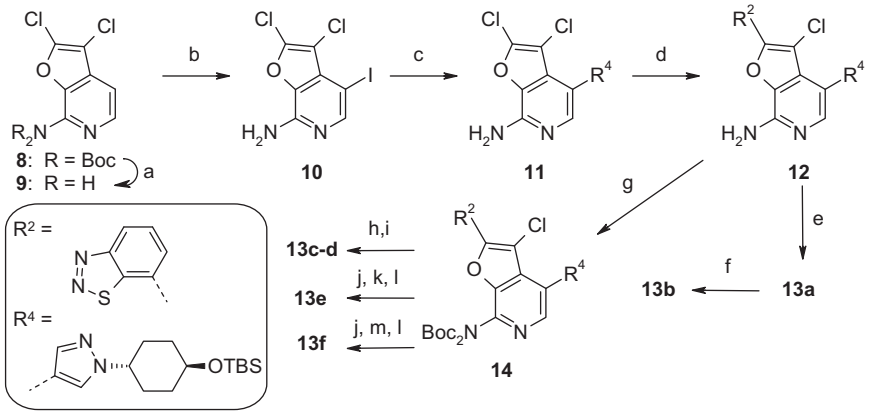

Scheme 2. Preparation of 3-substituted analogs **13**. Reagents and conditions: (a) 4 N HCl in 1,4-dioxane, 55 °C (68%); (b) NIS, MeCN, 60 °C (41%); (c) R^4-B(pin), $PdCl_2dppf$, K_2CO_3, 1,4-dioxane/H_2O, 75 °C (51%); (d) R^2-B(pin), $Pd(PPh_3)_4$, Na_2CO_3, 1,4-dioxane/H_2O, 120 °C, μW; (e) concd HCl, 40 °C (50%, 2 steps); (f) $Zn(CN)_2$, $Pd(PPh_3)_4$, 1,4-dioxane/DMF, 140 °C, μW (12%); (g) Boc_2O, DMAP, DCM, rt (79%); (h) Ar-B(pin), Pd_2dba_3, XPhos, K_3PO_4, 1,4-dioxane/H_2O, 100 °C, μW; (i) 4 N HCl in 1,4-dioxane, MeOH, rt; (j) vinyl-B(pin), Pd_2dba_3, XPhos, K_3PO_4, 1,4-dioxane/H_2O, 100 °C, μW (69%); (k) (i) O_3, DCM, (ii) $NaBH_4$ (50%); (l) (i) DeoxoFluor, DCM, 35 °C, (ii) 4 N HCl in 1,4-dioxane, 70 °C; (m) (i) O_3, DCM, (ii) PPh_3 (69%).

Table 4
SAR of 3-substitutions

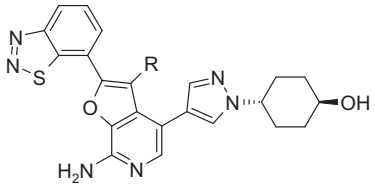

Compd	R	LLE[a]	IC_{50}[b] (μM)				ER[g]	
			TAK1[c]	pJNK[d]	pHH3[e]	pKDR[f]	Mouse	Human
1e	H	6.3	0.009	0.015	0.16	0.65	0.63	0.48
13a	Cl	5.1	0.028	0.018	6.5	>20	0.39	0.40
13b	CN	5.1	0.16	0.017	>10	>20	0.43	0.38
13c		4.8	0.11	0.13	6.9	8.2	0.48	0.41
13d		5.5	0.031	0.043	1.7	0.76	0.53	0.55
13e	CH_2F	5.7	0.017	0.045	1.5	18.3	0.43	0.49
13f	CHF_2	5.6	0.014	0.020	1.7	>20	0.39	0.48

[a] LLE = TAK1 pK_i – c$\log D_{7.4}$. See Ref. 1 for details.
[b] Values are the mean of ⩾2 experiments; NT = not tested.
[c] Biochemical ALPHAScreen assay with TAK1–TAB1 fusion protein in the presence of 100 μM ATP.
[d] Inhibition of JNK phosphorylation in TNFα-stimulated HCT-116 cells.
[e] Inhibition of histone H3 (HH3) S10 phosphorylation in HT-29 cells.
[f] Inhibition of KDR autophosphorylation in HEK293/KDR cells.
[g] Extraction ratio (ER) in mouse and human liver microsomes.

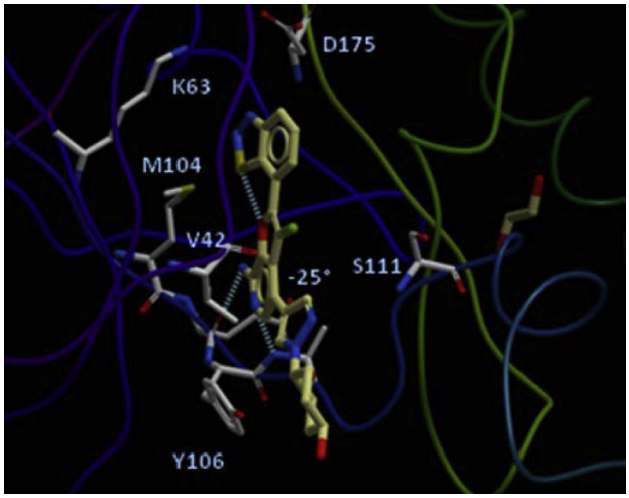

Figure 3. Single crystal X-ray structure of compound **13a** bound to TAK1–TAB1 fusion protein (2.5 Å resolution); PDB entry code 4L53. Key hydrogen bonds, internal contacts, and dihedral angles are displayed.

substantially reduced iv clearance, with correspondingly excellent oral exposure and bioavailability, and demonstrated oral PK curves absent the late concentration increases which would be indicative of enterohepatic recycling. At a higher 100 mg/kg dose, **13a** showed less than dose-proportional increases in C_{max} and $AUC_{0-\infty}$ and decreased bioavailability, indicating solubility- and/or permeability-limited absorption at the higher dose.

Now that suitable tool compounds had been identified, we next turned to an evaluation of compound **13a** (hereafter referred to as ABC-FP[13]) in an in vivo model of ovarian cancer (Fig. 4). Although until this point we had been screening compounds in vitro vs the HCT-116 colorectal carcinoma cell line, a parallel ongoing analysis

Table 5
Mouse pharmacokinetic parameters for selected compounds

Route	Parameters	**13a**	**13f**
iv[a]	Cl (mL/min/kg)	20	10
	$t_{½}$ (h)	2.1	1.8
	$AUC_{0-\infty}$ (ng h/mL)	1698	3440
	V_{ss} (L/kg)	2.1	1.0
p.o.[b]	C_{max} (μM)	3.8	18.6
	$AUC_{0-\infty}$ (ng h/mL)	8774	33,710
	F (%)	52	98
p.o.[c]	C_{max} (μM)	7.1	NT
	$AUC_{0-\infty}$ (ng h/mL)	26780	NT
	F (%)	32	NT

[a] iv PK dosed at 2 mg/kg.
[b] p.o. PK dosed at 20 mg/kg.
[c] p.o. PK dosed at 100 mg/kg. NT = not tested.

of tumor xenograft samples showed high in vivo levels of the activating cytokine TNFα in the clear cell ovarian line TOV21G. Cellular mechanistic inhibition of pJNK by ABC-FP in TOV21G (IC_{50} = 0.028 - μM) was comparable to that seen in HCT-116. It was thus postulated that the TOV21G cell line would be a more robust model for the in vivo evaluation of TAK1 inhibitors than HCT-116. CD-1 nude mice bearing subcutaneous TOV21G tumor xenografts were treated with 100 mg/kg of ABC-FP daily for 14 days. Over the dosing interval, ABC-FP showed a calculated 62% tumor growth inhibition on day 15, indicating some potential for a TAK1 inhibitor to be useful in the treatment of ovarian cancer.

In summary, we have evolved a series of potent but relatively poorly kinase selective 7-aminofuro[2,3-*c*]pyridine inhibitors of TAK1 with poor pharmacokinetics into more selective inhibitors with excellent oral exposure. These efforts culminated in the demonstration of in vivo efficacy for compound ABC-FP in an ovarian cancer model. Structure-based fine tuning of steric and conformational properties allowed for the exploitation of relatively small

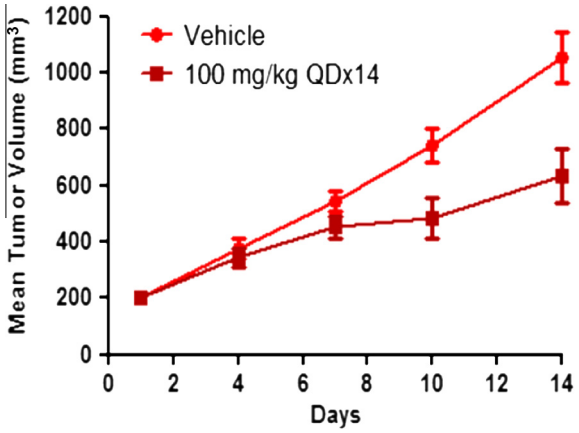

Figure 4. Tumor growth inhibition of compound ABC-FP in TOV21G xenograft model.

differences in the kinase active sites to achieve useful levels of Aurora B and KDR cellular kinase selectivity. Kinase selectivity improvements ultimately came along a more subtle path after the more obvious avenues had failed. In conjunction, analysis of in vitro metabolite profiling data enabled the design of compounds with lower clearance through the use of the same single substitution used for kinase selectivity. We were further able to rapidly execute the synthesis of these compounds by taking advantage of an observed by-product in the core synthetic route. Although the final structures resulting from this effort were only slightly removed from the starting points, they were arrived at through a carefully-reasoned and systematically evaluated approach. Further profiling of the in vitro and in vivo pharmacology of ABC-FP will be reported in due course.

Acknowledgments

We would like to thank Ms. Viorica Lazarescu and Dr. Yingjie Li for analytical support, Proteros Biostructures for solving the crystal structure of **13a** in complex with TAK1–TAB1 fusion protein, and Drs. Arno Steinig, Andrew Garton, and Maryland Franklin for helpful discussions. We also thank Janine Schwedes for technical assistance in the manuscript revisions.

References and notes

1. Hornberger, K.R.; Berger, D.M.; Crew, A.P.; Dong, H.; Kleinberg, A.; Li, A.-H.; Medeiros, M.R.; Mulvihill, M.J.; Siu, K.; Tarrant, J.; Wang, J.; Weng, F.; Wilde, V.L.; Albertella, M.; Bittner, M.; Cooke, A.; Gray, M.J.; Maresca, P.; May, E.; Meyn, P.; Peick Jr., W.; Romashko, D.; Tanowitz, M.; Tokar, B. *Bioorg. Med. Chem. Lett.* **2013**, *23*, 4517.
2. Manning, G.; Whyte, D. B.; Martinez, R.; Hunter, T.; Sudarsanam, S. *Science* **2002**, *298*, 1912.
3. Knight, Z. A.; Shokat, K. M. *Chem. Biol.* **2005**, *12*, 621.
4. Smyth, L. A.; Collins, I. *J. Chem. Biol.* **2009**, *2*, 131.
5. Dar, A. A.; Goff, L. W.; Majid, S.; Berlin, J.; El-Rifai, W. *Mol. Cancer Ther.* **2010**, *9*, 268.
6. Korpanty, G.; Smyth, E. *Curr. Pharm. Des.* **2012**, *18*, 2680.
7. Eskens, F. A. L. M.; Verweij, J. *Eur. J. Cancer* **2006**, *42*, 3127.
8. (a) Leeson, P. D.; Springthorpe, B. *Nat. Rev. Drug Disc.* **2007**, *6*, 881; (b) Edwards, M. P.; Price, D. A. *Ann. Rep. Med. Chem.* **2010**, *45*, 381. See footnote 15 of ref. 1 for details of our computational method.
9. Davies, N. M.; Takemoto, J. K.; Brocks, D. R.; Yáñez, J. A. *Clin. Pharmacokinet.* **2010**, *49*, 351.
10. (a) http://www.optibrium.com/stardrop (accessed April 2, 2013); For details of the underlying computational method, see: (b) Jones, J. P.; Mysinger, M.; Korzekwa, K. R. *Drug Metab. Dispos.* **2002**, *30*, 7.
11. Synthesis conditions to increase the yield of **8** from the originally reported 18% by increasing the equivalents of base and Cl3CCCl3 have been developed and will be reported in due course.
12. Billingsley, K. L.; Anderson, K. W.; Buchwald, S. L. *Angew. Chem., Int. Ed.* **2006**, *45*, 3484.
13. ABC-FP = *trans*-4-{4-[7-**a**mino-2-(1,2,3-**b**enzothiadiazol-7-yl)-3-**c**hloro**f**uro[2,3-c]**p**yridin-4-yl]-1*H*-pyrazol-1-yl}cyclohexanol.